Local hydraulic resistance in heterogeneous porous media

Quirine Krol[1], Itzhak Fouxon [1,2], Pascal Corso [1], Markus Holzner [1,3,4]

[1]ETH Zurich, Stefano Franscini-Platz 5, 8093 Zurich, Switzerland

[2]Department of Computational Science and Engineering, Yonsei University, Seoul 120-749, South Korea

[3]Swiss Federal Institute for Water Science and Technology EAWAG

[4]Swiss Federal Institute for Forest, Snow and Landscape Research WSL

Corresponding author: Quirine Krol, `quirine.krol@protonmail.com`

Abstract

We examine the validity of the commonly used Hagen-Poiseuille model of local resistance of porous media using direct numerical simulations. We provide theoretical arguments that highlight possible limitations of this model and formulate a new constitutive model that is based on the circularity of iso-pressure surfaces. We compare the performance of both models on three different three-dimensional artificial porous media. We show that the new model improves the root-mean-squared-relative error from 59%, 48% and 32% for the HP model to 12%, 14% and 18% for the three porous media respectively. We anticipate that our approach may find broad application in network models of porous media that are typically build from 3D images with intricate pore geometries.

1 Introduction

Porous media flow is important for a wide range of applications in nature and technology, spanning from groundwater remediation and oil recovery to packed bed reactors and particle filters. In these flows, the highly complex and three-dimensional pore geometries give rise to complicated pore velocity fields that form the backbone for transport, mixing and chemical reaction processes. Detailed knowledge of these velocity fields is important for the modelling of effective parameters, most notably the permeability and the prediction of transport in porous media (Bear, 1972; Scheidegger, 1974). Despite its importance and extensive research, however, the relation between geometrical features of porous media and the resulting flow is still not fully understood.

Given that detailed knowledge of geometrical features of porous media is often unavailable, the classical flow modeling approach has been to represent the porous medium as a lattice of circular tubes that represent the pore network (Scheidegger, 1974). The flow in the tubes is assumed uniform and the velocity profile parabolic. While this is a rather crude approximation of the real geometry and flow behaviors, it has provided useful predictions for flow and transport. Early studies have modelled velocity distributions (Haring & Greenkorn, 1970), permeability (Fatt, 1956; Katz & Thompson, 1986) and particle dispersion (Saffman, 1959) based on bulk statistics of the medium geometry such as pore size distributions. These early studies have spurred many subsequent works on statistical pore scale models e.g. Dullien (1975); Kutsovsky et al. (1996); Maier et al. (1999); de Anna et al. (2017) and Dentz et al. (2018). The second class of models that hinges on the simplified lattice representation of porous media are the so-called pore network

models (Thompson & Fogler, 1997). For both classes of models, the simplified modelling of local hydraulic resistance of individual pores based on Hagen-Poiseuille is a central element.

Many authors tried to relate the statistics of pore velocity to statistics of pore geometry represented by e.g. the local pore radius and the connectivity between pores. For example, one of the simplest models is the so-called *capillary bundle* model, in which the porous medium is conceptualized as a parallel arrangement of capillaries with given pore sizes (Scheidegger, 1974). Extensions of this model include parallel arrangements of wavy tubes (Le Borgne et al., 2011). These simple models are not appropriate for complex porous media, for which the network aspect is important. That is, in general, the connectivity between pores cannot be neglected and the concept of the linear pore breaks down (Dentz et al., 2018). An ad-hoc model that conceptualizes flow in porous media as a system of serial and parallel pore arrangements can be found in Holzner et al. (2015), and the resulting dispersion of tracers was predicted by Fouxon and Holzner (2016). Siena et al. (2014) and Hyman et al. (2012) statistically related velocity distributions to pore size distributions of statistically generated 3D porous media. Based on direct numerical simulations in 2D porous media composed of disks, de Anna et al. (2017) showed that the low velocity tail of the pore velocity distribution is governed by local pore size. This is a notable result as it suggests that the slow flow velocities are not strongly dependent on the connectivity between pores. Alim et al. (2017) showed that pore velocity distributions are governed by local correlations of pore sizes that organize flux ratios at pore junctions, while pore size itself was a poor predictor of flux ratios. They simplified two-dimensional porous medium flow by a network of tubes with varying diameter and the flow within each tube was calculated by solving for Kirchoffs circuit law for two-dimensional Poiseuille flow within the tubes of rectangular cross section. Even though using tubes with varying diameter is a refinement compared to simpler models with tubes of constant diameter, the simplification with respect to real geometries is still strong. Despite this, a comparison of simulation results with the experimentally obtained velocity distribution in a two-dimensional micromodel composed of pillars showed reasonable agreement (Alim et al., 2017). As mentioned, the statistical models in these works are based on the concept that local velocity profiles are parabolic. Some recent papers provided qualitative examples comparing pore velocity profiles to a parabola that suggest the assumption may be reasonable (de Anna et al., 2017; Dentz et al., 2018) and some evidence

is provided by the comparison between simulations and experiments by Alim et al. (2017). However, a rigorous assessment of local hydraulic resistance in three-dimensional pore geometries is still missing in the literature.

With the advent of experimental techniques like micro-computed tomography there is now access to impressive details of three dimensional porous media architectures. Even though today's computing facilities make it possible to solve flow and transport with unprecedented accuracy in these complex geometries using direct numerical simulations, this approach is only feasible in small domains. Simple models that reduce the full complexity of real porous media are still needed. A lattice representation is the standard approach in so-called pore network models in which a Kirchhoff-type system of equations is solved to model single or multiphase porous medium flows (Thompson & Fogler, 1997) especially in absence of a detailed microstructure. The lattice is usually constructed based on data from experimental pore scale characterization measurements, e.g. imaging or mercury intrusion porosimetry. These pore network models are a valuable tool for understanding meso-scale phenomena, linking single pore processes and continuum porous media used in engineering (Xiong et al., 2016). Besides a sound network construction approach that mimics the real media, another critical aspect for the accuracy of modeling is the representation of local hydraulic resistance in the pores.

In this paper we start with a theoretical background where we define local pores based on consecutive iso-pressure surfaces, followed by a new model for the local hydraulic conductivity. In the methods section we describe our numerical experiment consisting of direct numerical simulations (DNS) from which we obtain local velocity and pressure data in heterogeneous porous media. Based on a post-processing of the DNS data we can extract the local hydraulic conductivity of a local pore. In the results we compare the measured hydraulic resistances to the Hagen-Poiseuille model and to the newly formulated model based a local shape parameter circularity. In the discussion we treat the limitations and extrapolations of the newly proposed model. In the final chapter we provide our conclusions.

2 Theoretical Background

For low Reynolds numbers and incompressible flow, the local flow in a porous media is described by the Stokes equations,

$$\nabla p = \mu \nabla^2 \mathbf{u}, \quad \nabla \cdot \mathbf{u} = 0 \tag{1}$$

with pressure p and velocity $\mathbf{u}$ and dynamic viscosity μ. For an arbitrary volume $\mathcal{V}$ in a porous media, enclosed by surface $\partial \mathcal{V}$ given by two iso-pressure surfaces $\mathcal{S}_{p_1}$ and $\mathcal{S}_{p_2}$ and solid-liquid surface boundary Γ, we can write down the integral form of the Stokes equations using the divergence theorem.

$$\int_{\mathcal{V}} \left(\mathbf{u} \cdot \nabla p - \mu \mathbf{u} \cdot \nabla^2 \mathbf{u} \right) dV = \int_{\partial \mathcal{V}} p\, \mathbf{u} \cdot \mathbf{n}\, dS - \mu \int_{\partial \mathcal{V}} \mathbf{u} \cdot (\nabla \otimes \mathbf{u}) \mathbf{n}\, dS + \mu \int_{\mathcal{V}} (\nabla \otimes \mathbf{u})^2 dV = 0, \tag{2}$$

with $\mathbf{n}$ the normal vector pointing outwards of surface ∂V, and $\otimes$ the dyadic product. Given that at the porous media boundary domain Γ we have a no-slip condition $\mathbf{u} = 0$ we can write

$$Q\Delta p = -\mu \int_{S_{p_1} + S_{p_2}} \mathbf{u} \cdot (\nabla \otimes \mathbf{u}) \mathbf{n}\, dS + \mu \int_{\mathcal{V}} (\nabla \otimes \mathbf{u})^2 dV, \tag{3}$$

with the total flux through any cross section defined by

$$Q = \int \mathbf{u} \cdot \mathbf{n}\, dS. \tag{4}$$

Here we introduce the notion of disconnected iso-pressure surface $\mathcal{S}_i(p)$ for a given pressure value p. Iso-pressure surfaces are usually disconnected because they exist in the fluid domain only and are thus interrupted by the solid phase of the media. The first term of Eq. (2), the boundary term, will be less significant when the total volume V is enlarged by increasing δp. Furthermore, when we have saturated conditions, the complete pore space can be compartmentalized in a network of enclosed volumes $V_i(p_i, p_i + \delta p_i)$, which we will later call pores. We have assessed the relevance of the boundary term to $Q\Delta p$ for ten pores in the SI. We found that they contribute generally below 5% for the shortest available pores to below 1% for average size pores. Therefore it is reasonable to estimate Eq. (2) by

$$Q\Delta p \approx \mu \int (\nabla \otimes \mathbf{u})^2 dV. \tag{5}$$

In the following we apply a decomposition of the velocity vector $\mathbf{u} = u_p \hat{\mathbf{p}} + u_r \hat{\mathbf{r}}$ with $\hat{\mathbf{p}} = \nabla p / |\nabla p|$ (longitudinal direction in respect to the flow) and $\hat{\mathbf{p}}$ perpendicular to $\hat{\mathbf{r}}$ (transversal direction in respect to the flow). We assume that the most important
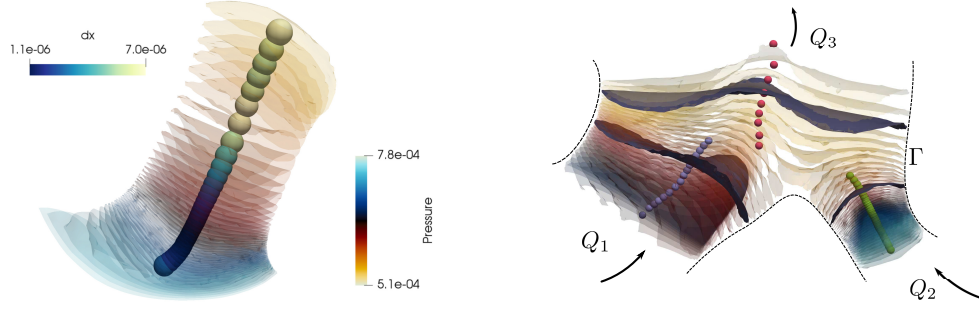
Figure 1: Left: A visualization of a collection of consecutive iso-pressure surfaces comprising one pore, including the center of mass of the iso-pressure surfaces indicated by the spheres. The color code of the spheres is given by the distance between the average coordinates between two consecutive iso-pressure surfaces. Right: A visualization of a junction of three pores for which the total flux is conserved $Q_1 + Q_2 = Q_3$. This visualization is based on a subset of the DNS results of porous media #2

contributions to the viscous dissipation tensor $\nabla_i u_j$ are given by $\nabla_i u_p$ i.e. $\nabla_i u_r \ll \nabla_i u_p$. Also this assumption has been verified in the supplementary information (SI) for the porous media that we have used below and leads to

$$|\nabla_i u_j|^2 \approx |\nabla_r u_p|^2 + |\nabla_p u_p|^2 \,. \tag{6}$$

Here the first term is expected to be more important for gradually varying pore geometries since gradients in the velocity in the longitudinal direction are usually much lower than in transverse direction. Equations (1)-(6) are valid for arbitrary volumes V. When we consider viscous dissipation in an *infinitesimal* volume dV enclosed by $\mathcal{S}(p), \mathcal{S}(p+\delta p)$ (with respective areas $A(p), A(p+\delta p)$), separated by average distance dx defined by $dV = A(p)dx$, we can estimate (analogous to Mortensen et al. (2005)) the average value of the first term of Eq. (6) by

$$|\nabla_r u_p|^2 = 8\pi \left(\alpha_0 + \alpha_1 \mathcal{C}\right) \frac{Q^2}{A^3} \quad , \tag{7}$$

with circularity parameter $\mathcal{C} = \mathcal{L}^2/4\pi A(p)$ with perimeter $\mathcal{L} = \int_{\partial \mathcal{S}(p)} dl$. The circularity parameter is related to the compactness factor $C = \mathcal{C}/4\pi$ in (Mortensen et al., 2005), and for HP flow it is equal to one. The coefficients α_0 and α_1 can be calculated (in first order of circularity) analytically or numerically for simple shapes of the iso-pressure

–6–

surfaces, such as squares, triangles, or a perturbation of a sphere by spherical harmonics (Mortensen et al., 2005). For heterogeneous media the class of shapes are generally unknown and not symmetric, and therefore α_0 and α_1 are expected to be intrinsically dependent on the pore geometry and therefore to change from pore to pore.

For the second, longitudinal term, we can assume that the total flux Q remains constant for $p \rightarrow p+dp$, and the change of the velocity in longitudinal direction is caused by a change in cross-sectional area $A(p) \rightarrow A(p+\delta p)$. We estimate u_p by the total flux Q/A, i.e.

$$|\nabla_p u_p|^2 = 8\pi \alpha_2 \frac{Q^2}{A^4} \left| \frac{dA}{dx} \right|^2 , \tag{8}$$

with proportionality factor α_2. Again, α_2 is intrinsically dependent on pore geometry and changes from pore to pore. We combine the two expressions Eq. (7) and Eq. (8) with Eq. (5) into

$$\frac{dp}{dx} = 8\pi\mu \frac{Q(p)}{A(p)^2} f\left(\alpha_i, \mathcal{S}(p) \right), \tag{9}$$

with

$$f\left(\alpha_i, \mathcal{S}(p) \right) = \alpha_0 + \alpha_1 \mathcal{C} + \alpha_2 \frac{1}{A} \left| \frac{dA}{dx} \right|^2 . \tag{10}$$

This parametrization is consistent with the Hagen-Poiseuille equation for pipe geometries $f(\alpha_i) \rightarrow 1$, for which the local infinitesimal pressure gradient is given by

$$\frac{dp}{dx} = 8\pi\mu \frac{Q}{A^2} . \tag{11}$$

As long as the total flux Q remains constant and $dV = Adx$ remains valid, Eq. (9) can be integrated over Δp. We define a pore by the integrated volume, bound by iso-pressure surfaces $\mathcal{S}_i(p)$, $\mathcal{S}_j(p + \Delta p)$ and the porous media boundary. The hydraulic resistance of a pore is then given by $\mathcal{R} = \frac{\Delta p}{Q}$. The right-hand side of Eq. (5) gives us therefore a statistical model for the hydraulic resistance $\mathcal{R}_m$ is given by

$$\mathcal{R}_m = 8\pi\mu \int_0^{L_{\text{eff}}} \frac{1}{A^2} f\left(\alpha_i, \mathcal{S}(p) \right) dx, \tag{12}$$

with $L_{\text{eff}} = \int dx$ the total effective length of the pore. When the geometry of a media is given by a long pipe, the hydraulic resistance is given by the Hagen-Poiseuille (HP) model $\mathcal{R}_{\text{HP}}$, given by $\mathcal{R}_m(f \rightarrow 1)$. The HP model therefore only depends on the cross-sectional area $A(p)$.
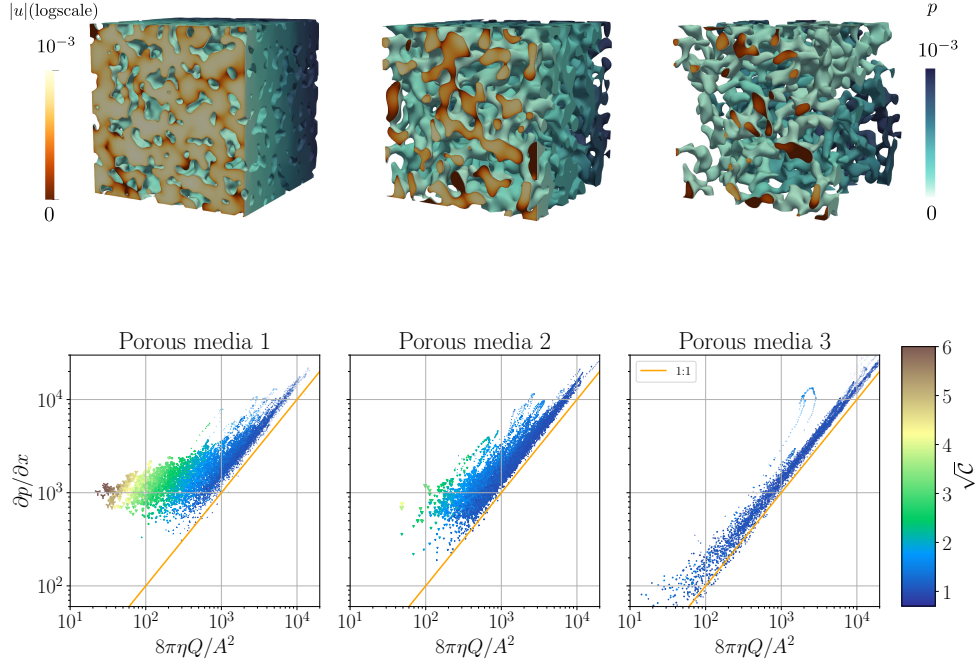
Figure 2: Top: A visualization of the velocity field $|u|$ and pressure field p in the pore space of the three porous media used in this study. Bottom: Measurements of local pressure drop versus the Hagen-Poiseuille model given by Eq. (11) for three different porous media. The color is given by averaged circularity $\mathcal{C}(p)_i$ and the marker size is scaled with the averaged area $A(p)_i$ of two consecutive iso-pressure surfaces $\mathcal{S}(p)_i, \mathcal{S}(p + \delta p)_j$.

3 Methods

To generate heterogeneous porous media we make use of the Gaussian Random Fields (GRF), which are increasingly used to represent realistic porous media (Liu et al., 2019). We used a fast Fourier transform and a spectral density function to generate GRF scalar functions (Teubner, 1991; Hyman et al., 2012; Siena et al., 2014). A threshold on the GRF function is used to define the porous media-fluid interface Γ with porosities $0.68, 0.34$ and 0.17 respectively. For details on the GRF functions and geometrical parameters such as average pore size and surface roughness are given in the SI. These porous media are used as input for direct numerical simulations (DNS, OpenFOAM v. 4.1, Weller et al. (1998)),

171   that solve the Stokes equations (Eq. 1) in the pore space. The boundary conditions are

172   defined at the inlet p_1 and outlet p_2 and a no-slip condition for the porous media-fluid

173   interface. A visualization of the three porous media is shown in Fig. 2. Next, a chain of

174   visualization toolkit (VTK) based image analysis techniques (Schroeder et al., 2006; Hern-

175   derson, 2007) is employed to extract iso-pressure surfaces $\mathcal{S}(p)$ and enumerate the dis-

176   connected areas identified as an iso-pressure patch $\mathcal{S}_i(p)$. This patch is part of a pore

177   and has a surface area $A_i(p)$, circularity $\mathcal{C}_i(p)$, center of 'mass' of iso-pressure surface $\mathbf{X}_i(p)$

178   and total flux $Q_i(p)$. For each $\mathcal{S}_i(p)$ we identify its closest neighbor $\mathcal{S}_j(p+\delta p)$. This neigh-

179   boring iso-pressure patch (building up a pore) is found by calculating the distance func-

180   tion $f_d(\mathbf{x}, \mathcal{S})$, between any given point $\mathbf{x} \in \mathcal{S}_i(p)$ and all iso-pressure patches $\mathcal{S}_k(p +$

181   $\delta p)$. This distance function is defined by

$$f_d\left(\mathbf{x}, \mathcal{S}\right) = \min\{\|\mathbf{x} - \mathbf{y}\|\} \mid \mathbf{y} \in \mathcal{S}. \tag{13}$$

182   for each i, k we define the averaged distance matrix

$$d_{i,k} = \frac{1}{A_i(p)} \int_{\mathcal{S}_i(p)} f_d(\mathbf{x}_i, \mathcal{S}_k(p + \delta p))\, dS_i. \tag{14}$$

183   The closest neighbor $\mathcal{S}_j(p + \delta p)$ is found by the minimum value of $d_{i,j} = \min\{\mathrm{d_{i,k}}\}$.

184   When δp is chosen sufficiently small the enclosed volume can be estimated by $V_i(p, \delta p) =$

185   $A_i dx_i \approx A_i d_{i,j}$. We use forward integration of consecutive patches until merging or split-

186   ting takes place. This is translated into constraints on flux conservation and an upper

187   bound for $d_{i,j}$. We noticed however that the distances between $\mathbf{X}_i(p)$ and $\mathbf{X}_j(p + \delta p)$

188   of two consecutive pores are more sensitive to topology changes, and are therefore used

189   instead. The precise values for these constraints can be found in the SI. A demonstra-

190   tion of the correct identification of pores by forward integration is shown in Fig. 1 (Right),

191   showing a merging of two pores. Although the proposed definition of individual pores

192   deals naturally with junctions, a straight forward pore-network implementation is still

193   missing. This is partly due to the exclusion of iso-pressure patches that are singular, and

194   have no neighboring patches due to rapid changing topologies. The percentages of ex-

195   cluded surface area patches are 18%, 26% and 2%, which, at least for the first two porous

196   media, prevents a continuous reconstruction of the network-topology. This is not an is-

197   sue for the present work which aims at validating the novel constitutive relation on the

198   level of individual pores and a continuous pore network is not required. However, for a

199   pore-network implementation of the approach to be applicable, this should be resolved

200   in future work.

The main challenge with the data format of the OpenFoam simulations is that it is unstructured, and the meshing is refined towards the boundary of the porous media Γ. Although this ensures that the geometry is accurately described and that the simulation converges, it also causes challenges in the extraction of $\mathcal{S}(p)$ by using a VTK contour filter. Since it is based on a threshold on p it breaks up the mesh close to Γ into many disconnected noisy area patches. These are removed by applying a filter on the area size of the patches, resulting in a reduction of total surface area of maximally 1%. Extracting circularity $\mathcal{C}_i(p)$ is achieved by applying a contour filter on $\mathcal{S}_i(p)$ with a threshold on the velocity of $|u| = 10^{-9}$ ms^{-1}, which is numerically zero.

For each of the three porous media we evaluate Eq. (9) for all consecutive iso-pressure pairs $\mathcal{S}_i(p)$. To obtain measured values for the resistance of a pore, we divide the total pressure difference Δp by the total flux Q. We fit Eq. (16), to all pores belonging to one porous media, yielding three sets of α_i.

4 Results

The result of the DNS for the three porous media is shown in Fig. 2. The Reynolds numbers are calculated by Re $\sim \ell_\mathrm{p} q/\nu$, with q the average flux through the porous media and ℓ_p the average pore size defined by the total porous media volume to total porous media interface ratio $\ell_p = 4\phi V/|\Gamma|$. For all porous media Re is smaller than 10^{-2}. In Fig. 2, bottom, the results of the infinitesimal pressure gradients versus the HP model (Eq. (11)) are shown. We observe that the HP model underestimates the pressure gradient by up to two orders of magnitude for the first porous media, to a relative good estimate for the third. We notice that $\mathcal{C}$ is the lowest for smallest pores, indicating that smaller iso-pressure surfaces are more circular than larger, more complex shaped iso-pressure surfaces. Besides the fact that the data covers different ranges we see no visual visual distinction between the three porous media, i.e. their data overlap and behave uniformly with respect to $\mathcal{C}$ and size A, see Fig. 3, top left.

For each porous media Eq. (9) has been fitted by minimizing the least-squared error independently to obtain estimates for α_i. The contribution of the term α_2 is insignificant for all three porous media and is reported in the SI. A simple fit, excluding α_2 resulted in three values for $\alpha_0 = 0.48, 0.52, 0.19$ and $\alpha_1 = 0.90, 0.87, 1.16$ for the corresponding porous media respectively. The result of the fitting is shown in Fig. 3 (top, right).

232   Using Eq. (9) with the fitted values for α_0 and α_1 ($\alpha_2 = 0$) we obtain a new model for

233   local pore resistances $\mathcal{R}_m$, Eq. (16), which performs much better than the HP model.

234   The result is shown in Fig. 3 (bottom, right). We notice that obtained values for α_1 are

235   underestimated by $1/\epsilon$ given that the circularity is overestimated by ϵ.

236   The Pearson correlation coefficients R^2 for all models of the resistances are higher

237   than 0.88. For the HP model the values for R^2 are given by $0.91, 0.88$ and 0.99. The co-

238   efficients R^2 of $\mathcal{R}_m$ are given by $0.97, 0.95$ and 0.99. The high values are caused by the

239   large domain size spanning several orders of magnitude. The deviations of $\mathcal{R}_{\mathrm{HP}}$ with the

240   measured values $\Delta p/Q$ are not uniform across the scales and therefore R^2 is not a re-

241   liable parameter when it comes to expressing the improvement over the HP model (Wilcox,

242   2009). We therefore calculated the reduction of the root-mean-squared-relative error (RM-

243   SRE) from $\mathcal{R}_{\mathrm{HP}}$ to $\mathcal{R}_{\mathrm{m}}$. For the first porous media we found a reduction in the RMSRE

244   from 59% to 12%, for the second from 46% to 13% and for the last from 31% to 15%.

245   We visually observe that the circumferences of the iso-pressure surfaces are not smooth

246   and lead to an overestimation of $\mathcal{C}_i(p)$. In the SI we have evaluated this error to be a fac-

247   tor $\epsilon = 1.15$, 1.11, 1.08 for the three porous media respectively. The origin of this er-

248   ror is the grid refinement near the boundary. Given that this is uniform throughout the

249   porous media, we expect the error to be similar for all $\mathcal{C}_i(p)$. Considering this observa-

250   tion and the fact that the last term in Eq. 10 is insignificant, it is interesting to test the

251   robustness of the linearity in $\mathcal{C}$ and the consistency of the function $f \rightarrow 1$ when $\mathcal{C} \rightarrow$

252   1. We introduce an alternative function g to f with two fit parameters α and β,

$$g(\mathcal{C}) = 1 - \alpha \left[1 - (\mathcal{C}/\epsilon)^\beta \right],\tag{15}$$

253   with a reduction factor $1/\epsilon$ for $\mathcal{C}$ to compensate for the known overestimation of $\mathcal{C}$. This

254   function is consistent with the HP model as long as $\beta = 1$. The fitting resulted in three

255   values for $\alpha = 0.45$, 0.58, 0.34, and $\beta = 1.09$, 1.05, 1.08. The latter suggesting that

256   non-linear contributions of $\mathcal{C}$ can be present but are expected to be relatively small. A

257   model including a quadratic term, reported in the SI, gives the same performance, but

258   with the danger of over-fitting. By using $g(\mathcal{C})$ the RMSREs are higher than for the model

259   resulting from fitting Eq. (16). This is reflected in a central spread of $\mathcal{R}_m$ around the

260   1 : 1 line, whilst with Eq. (15), the model predicts generally values above the 1 : 1 line.

261   The Pearson correlation coefficients of the uniform model are similar, given by $R^2 = 0.97$, 0.95

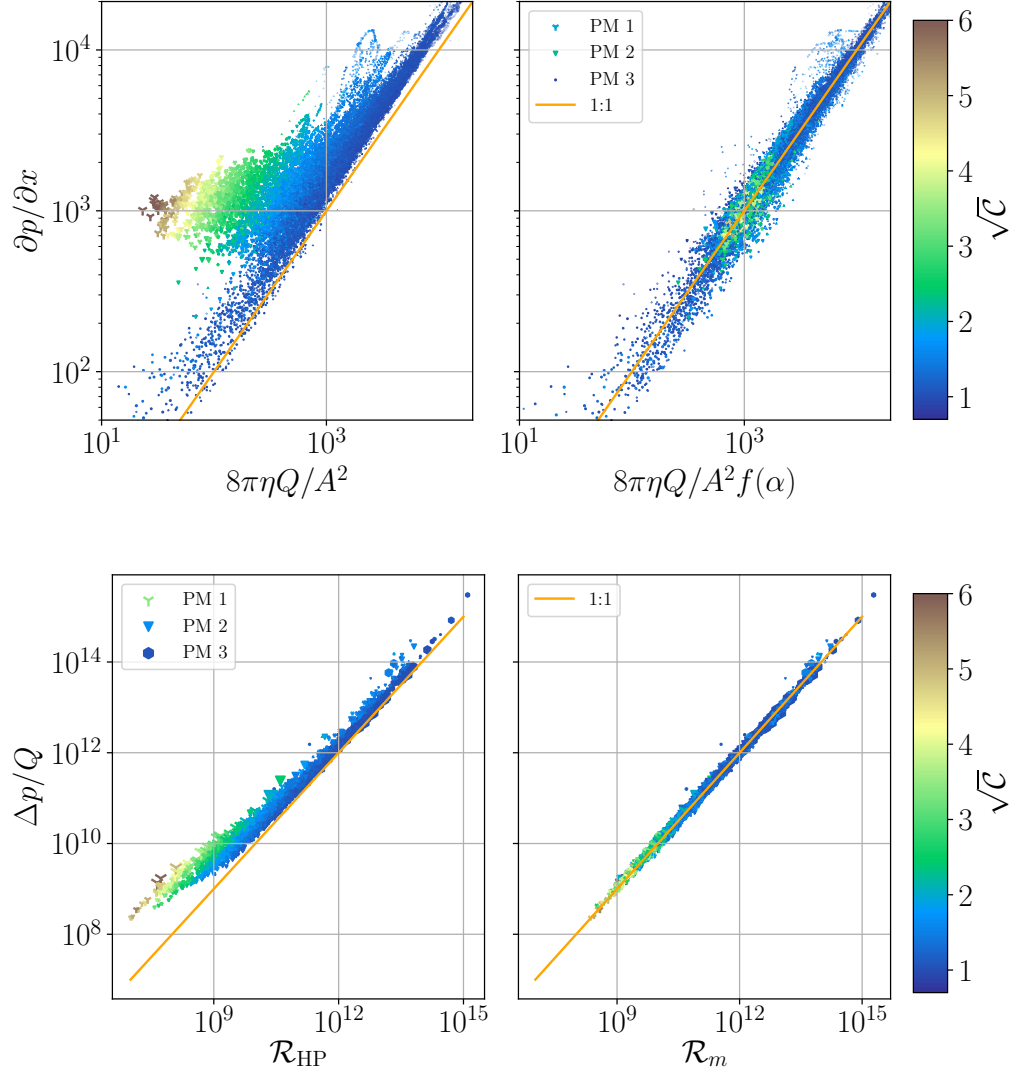Figure 3: Top left: Measured infinitesimal pressure gradient versus the infinitesimal pressure drop of a Hagen-Poiseuille model, i.e. $f(\alpha) \to 1$, for all three porous media combined. The marker size is scaled with square root of the averaged area $\sqrt{\overline{A}}$. Top right: Measured versus Modeled infinitesimal pressure gradient with $f(\alpha)$ fitted to Eq. (9) for each porous media separately. Bottom: The marker size is scaled by $N\sqrt{\overline{A}}$, with N the number of consecutive patches. Bottom left: Integrated pressure drop vs $\mathcal{R}_{HP}$ times the total Flux Q. Bottom right: Integrated pressure drop divided by the total Flux Q vs $\mathcal{R}_m$ (Eq. (16)).

262 and 0.99 indicating a similar performance. All models and their parameters including

263 performances are listed in the SI.

264 The range of local resistances in Fig. 3 (bottom) show that low resistances are cor-

265 related with high values for $\mathcal{C}$, and are poorly estimated by the HP model. These pores

266 are crucial for predicting preferential flow paths since they depend on the paths of least

267 resistances throughout a network. For this purpose we have computed the RMSRE weighted

268 by the mean flux. We found a reduction from $86\%, 60\%, 32\%$ for the HP model to $10\%, 12\%, 13\%$

269 for the new model for the three heterogeneous media respectively, which shows a remark-

270 able improvement for high flux pores.

5 Discussion

271

272 One of the most important findings is that the prediction of the resistance of a pore

273 by $\mathcal{R}_{\mathrm{HP}}$ is highly underestimated with an average RMSRE of 0.45. This is most pronounced

274 when the pores have a complex geometry, which are usually correlated with large pore

275 areas, see Fig. 3. An average underestimation of the resistances leads to an average over-

276 estimation of the mean fluxes in a network model. This will affect transport predictions

277 e.g. breakthrough times will be underestimated (Dentz et al., 2018). Network models

278 such as (Alim et al., 2017), often base their local resistances on the smallest distances

279 to the porous media boundary. In general this will underestimate the cross-sections and

280 therefore obtain higher resistances for the HP-based model, potentially reducing the er-

281 ror with respect to our HP model. Since anomalous diffusion has been correlated with

282 the degree of heterogeneity of the porous media, it is important that low flux regions are

283 included. The inaccurate representation of the low velocity regions of larger cross-sectional

284 areas will therefore contribute to poor estimates of anomalously long residence times.

285 Estimating these residence times properly is important because they underly non-Fickian

286 scaling behavior of the dispersion of flow tracers (Dentz et al., 2018; Dentz & Tartakovsky,

287 2006).

288 We expect that our main results are transferable to other media such as packed-

289 beads, sandstone and disordered media, since iso-pressure surfaces are quite heteroge-

290 neous even if grains are regular. In ordered and/or high porosity media we expect iso-

291 pressure surfaces that are highly connected, similar to porous media 1 in this paper, and

292 sometimes even consisting of a singular patch. In these cases extracting statistics can

be challenging. One possible strategy for separation of highly connected iso-pressure surfaces into smaller patches could be a watershed or Morse-Smale-Complex segmentation (Tierny et al., 2018).

One of the key observations of our work is the possibility of introducing a local geometric factor that provides for the ratio of pressure difference and mass flux in a given pore. The factor depends on the considered pore and not the rest of the complicated shape of the medium boundary. The non-triviality of this observation is made transparent by employing the boundary integral representation which is equivalent to the Stokes equations obeyed by the flow. The representation gives the flow as an integral over the medium surface where the points of the surface appear as sources that produce the flow as superposition. The "charge" of such sources is proportional to the stress tensor at the boundary and the flow that each charge induces in space is given by an appropriate Green's function, see e.g. (Pozrikidis, 1992). Our result demonstrates that contributions other than those from the boundary of the considered pore can be neglected in the superposition. The mechanism by which this occurs, consists of both screening effect and destructive interference between different pores. This deserves further studies which are beyond our scope here. We have used circularity, as a single measure for the shape of $\mathcal{S}(p)_i$, but to improve on this result it might be necessary to include other shape parameters such as curvature measures of $\mathcal{S}(p)_i$ and/or inclusion of a model for the boundary term (first term of Eq. 3), which however may lead to non-linear behavior in a circuit model.

Although a pore-network implementation is still missing due to the incomplete evaluation of all surface area patches, an alternative option is to use a statistical network representation based on our results. Given that the distributions of the resistances show similarity with a log-normal distribution (see SI), a pathway for a statistical network based on these distributions seems feasible.

6 Conclusion

We have proposed a new iso-pressure surface based definition for individual pores in heterogeneous porous media with the aim of measuring and modeling the local hydraulic resistance which can potentially be used in a pore-network model. This new definition uses the constant flux as constraint on the length of the pore. The definition of the pores allows us to estimate the local hydraulic resistance in terms of the viscous dis-

sipation tensor. This can be modeled by Eq. (16), with $\alpha_2 = 0$ resulting in

$$\mathcal{R} = 8\pi\mu \int_0^{L_{\text{eff}}} \frac{1}{A^2} \left(\alpha_0 + \alpha_1 \mathcal{C}\right) \, dx. \tag{16}$$

This model significantly improves the Hagen-Poiseuille model for heterogeneous media.

7 Data availability

The results of the DNS simulations and the results of the postprocessing on which the figures are based can accessed here (Krol, 2021).

Acknowledgments

References

Alim, K., Parsa, S., Weitz, D. A., & Brenner, M. P. (2017, October). Local Pore Size Correlations Determine Flow Distributions in Porous Media. *Phys. Rev. Lett.*, *119*(14), 144501. doi: 10.1103/PhysRevLett.119.144501

Bear, J. (1972). *Dynamics of fluids in porous media.*

de Anna, P., Quaife, B., Biros, G., & Juanes, R. (2017, December). Prediction of the low-velocity distribution from the pore structure in simple porous media. *Phys. Rev. Fluids*, *2*(12), 124103. doi: 10.1103/PhysRevFluids.2.124103

Dentz, M., Icardi, M., & Hidalgo, J. J. (2018, April). Mechanisms of dispersion in a porous medium. *Journal of Fluid Mechanics*, *841*, 851–882. doi: 10.1017/jfm .2018.120

Dentz, M., & Tartakovsky, D. M. (2006). Delay mechanisms of non-Fickian transport in heterogeneous media. *Geophysical Research Letters*, *33*(16). doi: 10 .1029/2006GL027054

Dullien, F. A. L. (1975, January). Single phase flow through porous media and pore structure. *The Chemical Engineering Journal*, *10*(1), 1–34. doi: 10.1016/0300 -9467(75)88013-0

Fatt, I. (1956, December). The Network Model of Porous Media. *Transactions of the AIME*, *207*(01), 144–181. doi: 10.2118/574-G

Fouxon, I., & Holzner, M. (2016, August). Solvable continuous-time random walk model of the motion of tracer particles through porous media. *Phys. Rev. E*, *94*(2), 022132. doi: 10.1103/PhysRevE.94.022132

Haring, R. E., & Greenkorn, R. A. (1970). A statistical model of a porous medium with nonuniform pores. *AIChE Journal*, *16*(3), 477–483. doi: 10.1002/aic .690160327

Hernderson, A. (2007). *ParaView Guide, A Parallel Visualization Application.*

Holzner, M., Morales, V. L., Willmann, M., & Dentz, M. (2015, July). Intermittent Lagrangian velocities and accelerations in three-dimensional porous medium flow. *Phys. Rev. E*, *92*(1), 013015. doi: 10.1103/PhysRevE.92.013015

Hyman, J. D., Smolarkiewicz, P. K., & Winter, C. L. (2012, November). Heterogeneities of flow in stochastically generated porous media. *Physical Review E*, *86*(5). doi: 10.1103/PhysRevE.86.056701

Katz, A. J., & Thompson, A. H. (1986, December). Quantitative prediction of permeability in porous rock. *Phys. Rev. B*, *34*(11), 8179–8181. doi: 10.1103/ PhysRevB.34.8179

Krol, Q. (2021). *Hydraulic resistance of pores in porous media using DNS of laminar flow.* EnviDat.

Kutsovsky, Y. E., Scriven, L. E., Davis, H. T., & Hammer, B. E. (1996, April). NMR imaging of velocity profiles and velocity distributions in bead packs. *Physics of Fluids*, *8*(4), 863–871. doi: 10.1063/1.868867

Le Borgne, T., Bolster, D., Dentz, M., de Anna, P., & Tartakovsky, A. (2011, December). Effective pore-scale dispersion upscaling with a correlated continuous time random walk approach: EFFECTIVE PORE-SCALE DISPERSION UPSCALING. *Water Resour. Res.*, *47*(12). doi: 10.1029/2011WR010457

Liu, Y., Li, J., Sun, S., & Yu, B. (2019, October). Advances in Gaussian random field generation: A review. *Comput Geosci*, *23*(5), 1011–1047. doi: 10.1007/ s10596-019-09867-y

Maier, R. S., Kroll, D. M., Davis, H. T., & Bernard, R. S. (1999, September). Simulation of Flow in Bidisperse Sphere Packings. *Journal of Colloid and Interface Science*, *217*(2), 341–347. doi: 10.1006/jcis.1999.6372

Mortensen, N. A., Okkels, F., & Bruus, H. (2005, May). Reexamination of Hagen-Poiseuille flow: Shape dependence of the hydraulic resistance in microchannels.

Physical Review E, *71*(5). doi: 10.1103/PhysRevE.71.057301

Pozrikidis, C. (1992). *Boundary Integral and Singularity Methods for Linearized Viscous Flow.* Cambridge: Cambridge University Press. doi: 10.1017/CBO9780511624124

Saffman, P. G. (1959, October). A theory of dispersion in a porous medium. *Journal of Fluid Mechanics*, *6*(3), 321–349. doi: 10.1017/S0022112059000672

Scheidegger, A. E. (1974). *The Physics of Flow Through Porous Media (3rd Edition).* University of Toronto Press.

Schroeder, W., Martin, K., & Lorensen, B. (2006). *The visualization toolkit: An object-oriented approach to 3D graphics* (4. ed ed.). Clifton Park, NY: Kitware, Inc.

Siena, M., Riva, M., Hyman, J. D., Winter, C. L., & Guadagnini, A. (2014). Relationship between pore size and velocity probability distributions in stochastically generated porous media. *Phys. Rev. E*, *89*(1), 013018. doi: 10.1103/PhysRevE.89.013018

Teubner, M. (1991). Level Surfaces of Gaussian Random Fields and Microemulsions. *EPL (Europhysics Letters)*, *14*(5), 403.

Thompson, K. E., & Fogler, H. S. (1997). Modeling flow in disordered packed beds from pore-scale fluid mechanics. *AIChE Journal*, *43*(6), 1377–1389. doi: 10.1002/aic.690430602

Tierny, J., Favelier, G., Levine, J. A., Gueunet, C., & Michaux, M. (2018, January). The Topology ToolKit. *IEEE Transactions on Visualization and Computer Graphics*, *24*(1), 832–842. doi: 10.1109/TVCG.2017.2743938

Weller, H. G., Tabor, G., Jasak, H., & Fureby, C. (1998, December). A tensorial approach to computational continuum mechanics using object-oriented techniques. *Computers in Physics*, *12*(6), 620. doi: 10.1063/1.168744

Wilcox, R. R. (2009, November). Comparing Pearson Correlations: Dealing with Heteroscedasticity and Nonnormality. *Communications in Statistics - Simulation and Computation*, *38*(10), 2220–2234. doi: 10.1080/03610910903289151

Xiong, Q., Baychev, T. G., & Jivkov, A. P. (2016, September). Review of pore network modelling of porous media: Experimental characterisations, network constructions and applications to reactive transport. *Journal of Contaminant Hydrology*, *192*, 101–117. doi: 10.1016/j.jconhyd.2016.07.002